Desalination and Water Treatment
www.deswater.com

doi: 10.5004/dwt.2018.21765

101 (2018) 291–300
January

Adsorptive removal of the hazardous anionic dye Congo red and mechanistic study of ZIF-8

Fangfang Xiao[a], Jianhua Cheng[a,b,*], Xiaoxiao Fan[b], Cao Yang[b], Yongyou Hu[a]

[a]*Ministry of Education Key Laboratory of Pollution Control and Ecological Remediation for Industrial Agglomeration Area, School of Environment and Energy, South China University of Technology, Guangzhou 510006, China, Tel. +86 20 38743625; Fax: +86 20 38743651; email: jhcheng@scut.edu.cn (J. Cheng), Tel. +8615602490483; email: 1447664536@qq.com (F. Xiao), Tel. +86 20 39380506; email: ppyyhu@scut.edu.cn (Y. Hu)*
[b]*South China Institute of Collaborative Innovation, Dongguan 523808, China, Tel. +8618814090493; email: 1315474816@qq.com (X. Fan), Tel. +86 18814116970; email: Aimee_yw@163.com (C. Yang)*

Received 2 June 2017; Accepted 5 December 2017

ABSTRACT

A metal–organic framework zeolitic imidazolate framework-8 (ZIF-8) nanosorbent was successfully prepared using a facile method under mild conditions. ZIF-8 was characterized using X-ray diffraction, Fourier transform infrared, scanning electron microscopy, X-ray photoelectron spectroscopy, and Brunauer–Emmet–Teller, and the material was used to remove Congo red (CR) from aqueous media. The adsorption kinetics, isotherms, and effects of pH and ionic strength were studied. The results showed that pseudo-second-order kinetics model and Langmuir isotherm matched well with CR adsorption on ZIF-8. The optimal conditions for CR removal occurred at neutral pH (6–8). Thermodynamics parameters of adsorption (free energy, enthalpy, and entropy) were also evaluated and indicated that the sorption process was spontaneous and exothermic. The possible mechanisms of CR adsorption onto ZIF-8 were attributed to electrostatic attractions, pore-filling effects, π–π interactions, and hydrogen bonding interactions. Regeneration of the adsorbent was also demonstrated using ethanol, and the adsorbent maintained good performance. The outstanding reusability and superior CR dye adsorbent capability of ZIF-8 demonstrated its potential application in wastewater treatment.

Keywords: ZIF-8; Nanosorbent; Adsorption; Congo red; Mechanisms

1. Introduction

Industrial wastewater, especially organic dye wastewater, contains many harmful substances that cause serious environmental problems. Dyes are water soluble and intensely colored substances and are used to color various substrates, including textiles, cosmetics, print media, food, and paper, and are used in other related industries [1]. Currently, more than 1×10^5 tons of commercial dyes are produced per year, and 10%–15% of that enters the environment through effluents, and azo dyes are nearly 70% of that [2]. The discharge of colored wastes not only affects the aesthetic nature of water for drinking and agricultural purposes but also disturbs the aquatic ecosystem by inhibiting sunlight and oxygen penetration of bodies of water, thus affecting aquatic life and the food web even when the colored wastes are in low concentrations [3].

Congo red (CR, 1-naphthalenesulfonic acid, 3,3′-(4,4′-biphenylene bis(azo)bis(4-amino-)disodium salt) is a benzidine-based anionic diazo dye and is one of the most widely used azo dyes in industry. The effluent is difficult to remove and decompose [2] because of its complex aromatic structure and high optical, thermal, chemically physical, and microbial stability.

* Corresponding author.

At present, numerous separation and removal techniques have been used to remove dye contaminants from wastewater, such as coagulation, membrane filtration, ultrasound irradiation, photo catalysis, oxidation, biological treatments, and adsorption [4]. Of these methods, adsorption is a widely used technique for removing dyes because of its low cost, high efficiency, environmental friendliness, simplicity of operation, and regeneration [1]. Many adsorbents, including active carbon, polymers, magnetic nanocomposites, and natural materials, have been used to remove dyes from wastewater [5]. However, these adsorbents have certain disadvantages, such as low adsorption capacity, complex preparation methods, and easy agglomeration, and these issues limit their applications. Hence, it is urgently necessary to develop a simple and efficient adsorbent for use in fields of both science and technology.

Recently, metal–organic frameworks (MOFs) have received considerable attention as a novel class of promising solid adsorbents in wastewater treatment because of their outstanding properties such as high surface areas, tunable pore sizes, versatile framework compositions, and structures [6]. There has been extensive research on the removal of various harmful compounds in the liquid phase using MOFs. MOFs can be modified for specific purposes, for example, surface modification, immobilization of functionalized materials, and grafting appropriate functional groups onto metal sites. Zhao et al. [7] successfully synthesized graphene oxide/metal–organic frameworks (GO/MOFs) using ultrasonic wave-assisted ball milling to achieve a respiration rate of 2,489 mg/g for CR, and this rate was much higher than that in previous reports. This proves that the ultrasonic wave-assisted ball milling material has good adsorption properties. Thanh et al. [8] synthesized a zeolitic imidazolate framework (ZIF-8) and iron-doped ZIF-8, which were used to remove Remazol Deep Black (RDB)RGB dye from aqueous solutions. Among various MOFs, ZIF-8, which is a rhombic dodecahedron formed by zinc ions and imidazolate ligands, have been found to be a potential adsorbent because of its ultrahigh porosity, excellent hydrothermal stability, hydrophobic nature, and economic synthesis [9]. ZIF-8 has been used for adsorptive removal of hazardous materials such as arsenic [10], p-arsanilic [11], phthalic acid, and diethyl phthalate [6]. However, only a few studies on adsorptive removal of dye have been reported.

In this work, ZIF-8 was prepared and characterized using X-ray diffraction (XRD), Fourier transform infrared (FTIR), Brunauer–Emmet–Teller (BET), scanning electron microscopy (SEM), and zeta potential analysis techniques. Removal of CR from aqueous solution was investigated using ZIF-8. Various adsorption parameters were evaluated, such as contact time, initial concentration of CR, temperature, ionic strength, and pH. In addition, adsorption kinetics, isotherms, and thermodynamic parameters were also investigated and are discussed in detail. Also, a possible mechanism of the adsorption process is proposed.

2. Experimental settings

2.1. Materials and reagents

Zinc nitrate hexahydrate [$Zn(NO_3)_2{\cdot}6H_2O$], 2-methylimidazole, sodium hydroxide (NaOH), hydrochloric acid (HCl), methanol, and CR were obtained. All of the solvents and reactants were analytical grade and were used without further purification.

2.2. Preparation and characterization of the adsorbents

ZIF-8 nanoparticles were prepared under normal conditions as described in a previous report [9]. Before adsorption, all of the adsorbents were dried overnight under vacuum at 100°C. XRD was carried out on an X-ray diffractometer (D8 ADVANCE, Bruker, Germany) over the 2θ range of 5°–55° using Cu-Kα radiation. FTIR (Nicolet 5700, Continuum, USA) spectra were obtained using Vector 33 KBr discs. SEM (Zeiss Merlin, Germany) was used to characterize the morphologies. The BET (NOVA 4200e, Quantachrome, USA) method was used to determine the specific surface areas, and the Barrett–Joyner–Halenda (BJH) method was used to estimate the pore size distributions and the pore volume. X-ray photoelectron spectroscopy (XPS, PHI X-tool, ULVAC-PHI, Japan) was used to examine the semi-quantitative surface chemical composition. Dynamic light scattering analysis (Zetasizer 3000HSA, Malvern, UK) was used to determine the zeta potentials. A Leici PHS-3C meter (Shanghai Precision and Scientific Instrument Co. Ltd., Shanghai) was used to analyze the solution pH.

2.3. Adsorption experiments

Batch adsorption experiments were conducted in a 250 mL Erlenmeyer flask containing 100 mL of working solution. ZIF-8 (0.02 g) was added to separate flasks and then shaken at 200 rpm and 25°C ± 1°C. During the experiment, an aliquot of the supernatant (4 mL) was taken from the solution at predetermined time intervals and analyzed. Adsorption isotherms were obtained over a CR concentration range of 10–500 mg L^{-1} at a certain temperature (25°C, 35°C, 45°C). UV–Vis spectroscopy was used to measure the absorbance of the solution at 497 nm to determine the CR concentrations. If the solution concentration was high, the solution was properly diluted. To investigate the effects of ionic strength, 10–100 mM NaCl or $CaCl_2$ solution were added to the solution. Different experiments were performed at pH values ranging from 2 to 12 to assess the effects of pH. The reusability of the adsorbents was determined in further adsorptions after recovering and washing the used adsorbents with 100 mL of water and 100 mL of ethanol three times each. The resulting suspension was mixed for 12 h using magnetic stirring at ambient temperature. The adsorbents were then recovered by further filtration, drying, and evacuation.

3. Results and discussion

3.1. Materials characterization

Fig. 1(a) shows a SEM image of ZIF-8 nanoparticles and reveals that the product consists of isometric nanoparticles with sharp edges. A statistical evaluation of 100 particles shows that the particle sizes are 50–100 nm and that the mean diameter is 72 nm (Fig. 1(b)). The N_2 adsorption–desorption isotherm of the ZIF-8 nanoparticles is shown in Fig. 1(c). The ZIF-8 nanoparticles have a microporous structure, and this is mainly because of the increase in the adsorption volume at

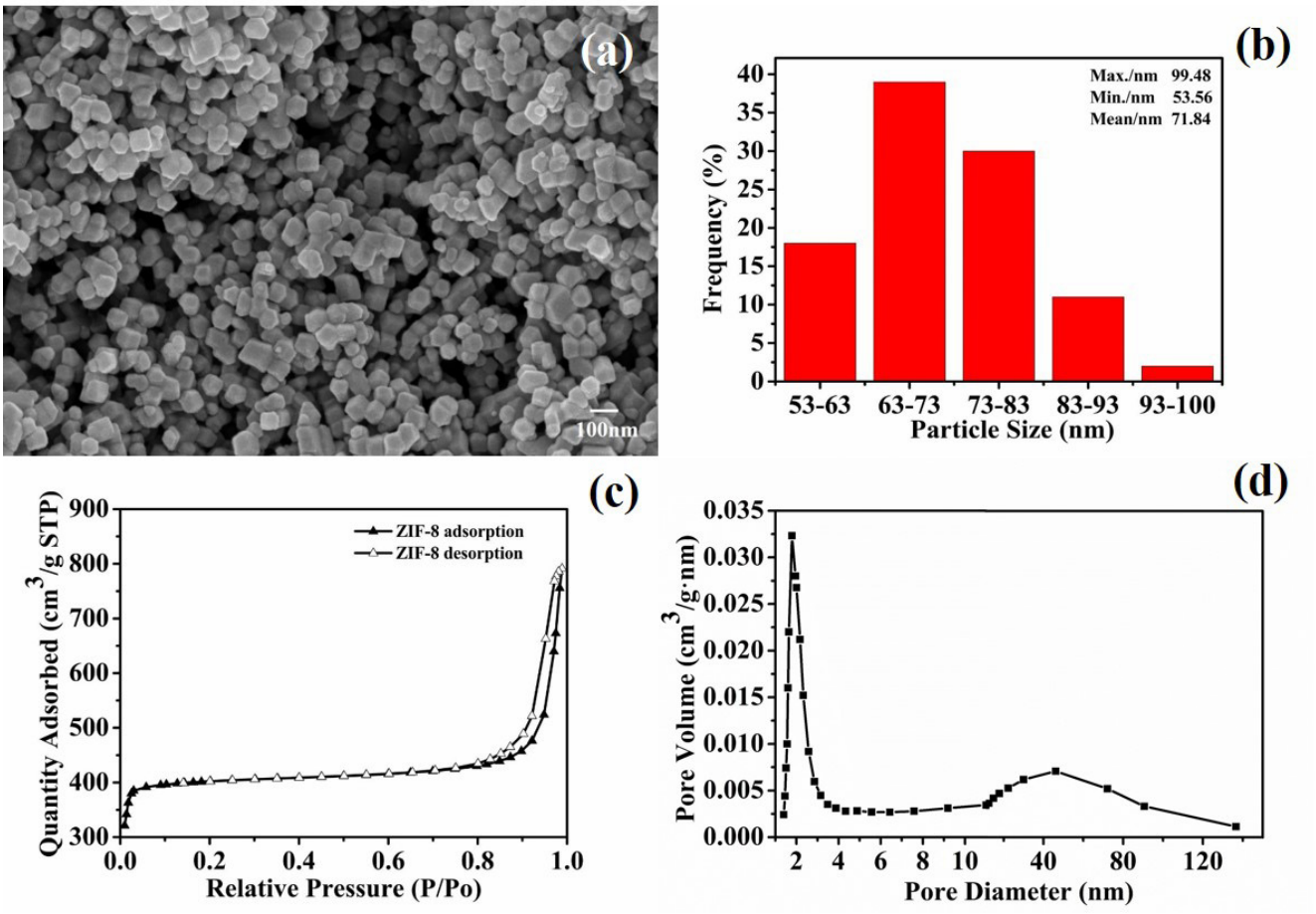

Fig. 1. (a) SEM image of ZIF-8 nanoparticles. (b) Statistical distribution of particle sizes. (c) Nitrogen adsorption isotherms at 77 K and (d) pore size distribution of ZIF-8.

low relative pressures. At large relative pressures ($P/P_0 > 0.8$), a hysteresis loop for the nitrogen isotherms was observed. This is because of the presence of meso/macroporosity between adjacent nanocrystals [9]. The BET specific surface area and total pore volume of the synthesized ZIF-8 nanoparticles were 1,345 m^2/g and 0.57 cm^3/g, respectively. This indicates a remarkable porous structure of the ZIF-8 nanoparticles, and Fig. 1(d) shows the pore size distribution curves of ZIF-8 in two viewing windows (about 1.4–2.9 nm and 12–90 nm).

3.2. Adsorption kinetics

Fig. 2(a) shows the effects of contact time on the adsorption capacity for CR adsorption at initial concentrations of 10, 40, and 100 mg L^{-1}. The adsorption capacity of CR increased with an increase in the adsorption time and initial concentration, and the equilibrium time increased with an increase in the initial concentration. Obviously, the adsorption process was faster at low initial concentration. When the CR concentration was low (10 mg L^{-1}), equilibrium was reached in 20 min with a saturation capacity of 50 mg g^{-1}, that is, CR was totally removed. At a CR concentration of 100 mg L^{-1}, the equilibrium time was prolonged to 90 min with a saturation capacity of 402 mg g^{-1}. This can be attributed to lower competition for the sorption surface sites at lower concentrations. At higher concentrations, the competition for the surface active sites is fierce, and consequently, lower sorption rates were obtained.

The adsorption data were fitted to different kinetics models such as the pseudo-first order (Fig. 2(c)), pseudo-second order (Fig. 2(b)), and intraparticle diffusion (Fig. 2(d)). These models can be expressed as:

$$\text{Pseudo-first-order model: } \ln\left(q_e - q_t\right) = \ln\left(q_e\right) - k_1 t \quad (1)$$

$$\text{Pseudo-second-order model: } \frac{t}{q_t} = \frac{1}{K_2 q_e} + \frac{t}{q_e} \quad (2)$$

$$\text{Intraparticle diffusion model: } q_t = Kt^{1/2} + C \quad (3)$$

where q_e and q_t (mg g^{-1}) are the uptake of CR at equilibrium and at time t (min), respectively. k_1 (min^{-1}) is the adsorption rate constant, k_2 (g mg^{-1} min^{-1}) is the rate constant of the second-order equation, and K (mg g^{-1} $min^{-1/2}$) is the intraparticle diffusion rate constant.

All of the parameters mentioned above were determined and are listed in Table 1. Higher values of R^2 (0.9984) are obtained for the pseudo-second-order kinetics model, and the calculated

equilibrium adsorption capacity (q_e) also agrees reasonably well with the experimental data using pseudo-second-order kinetics. These results show that the rates of that adsorption conform to pseudo-second-order kinetics.

The intraparticle diffusion model was used to provide information about whether external or internal diffusion is the dominant rate-limiting step during the adsorption process. As shown in Fig. 2(d), three linear plots were obtained for the adsorption process, and this implies that there were three diffusion steps in ZIF-8 nanoparticle adsorption [10]. The diffusion rate constants of the three steps are summarized in Table 2 and have an order of $K_1 > K_2 > K_3$ for CR. This means that the adsorption rate of external diffusion, which starts at the onset of the adsorption process, is the fastest. Therefore, it can be deduced that the present adsorption rates are mainly controlled by intraparticle diffusion.

3.3. Adsorption isotherms

For initial dye concentrations ranging from 10 to 500 mg L^{-1}, adsorption isotherms for ZIF-8 were obtained after adsorption for 12 h. The experimental data were fitted using two isotherm equations, namely, the Langmuir and Freundlich models. The equations for the Langmuir and Freundlich isotherm models are given in Eqs. (4) and (5) as follows:

$$\text{Langmuir: } \frac{C_e}{q_e} = \frac{C_e}{q_m} + \frac{1}{q_m b} \tag{4}$$

$$\text{Freundlich: } \log q_e = \log K_F + \frac{1}{n}\log C_e \tag{5}$$

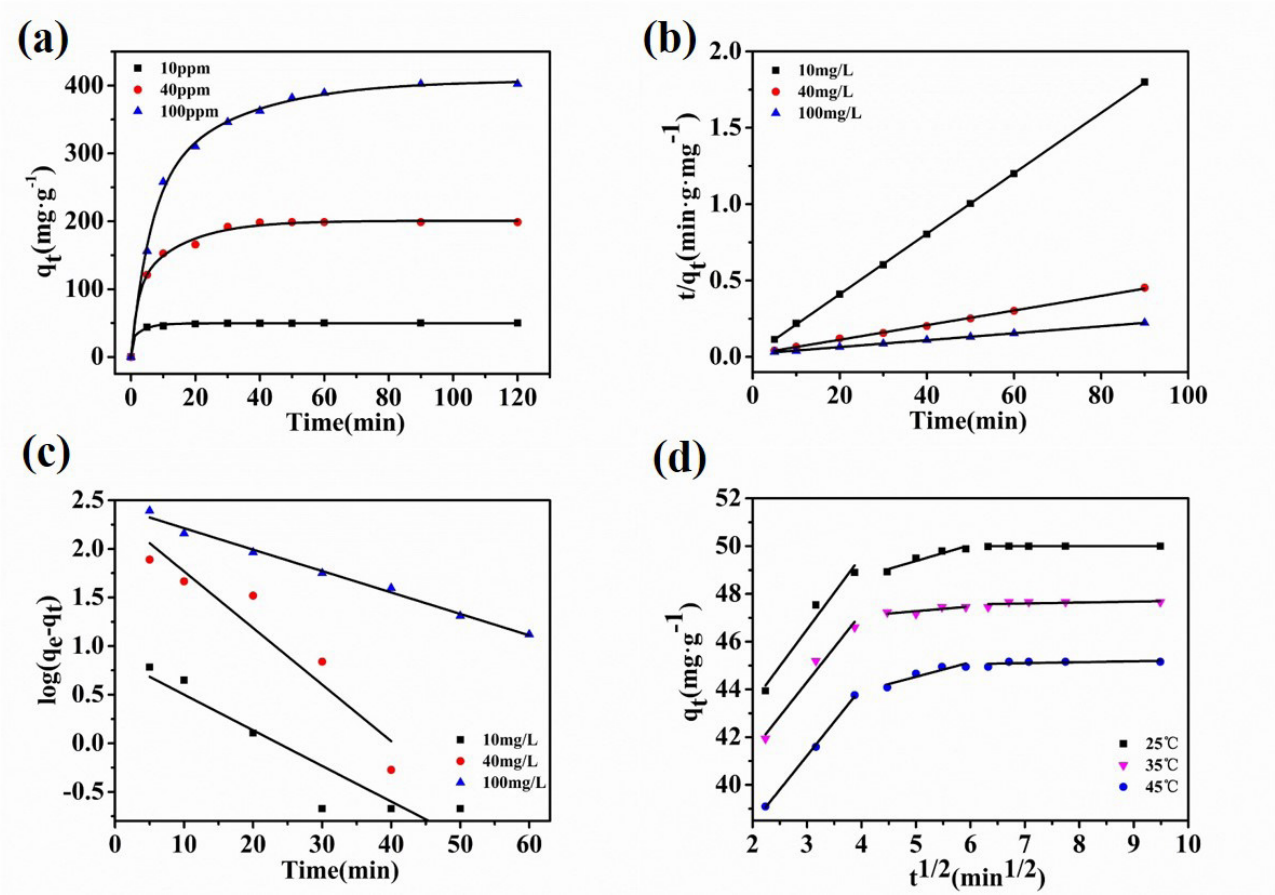

Fig. 2. (a) Effects of contact time on the adsorption capacity. Plots for (b) pseudo-second order, (c) pseudo-first order at 25°C, and (d) intraparticle diffusion for CR adsorption on ZIF-8. Solution pH = 6.7.

Table 1
Kinetics parameters for CR adsorption on ZIF-8

C_0 (mg·L^{-1})	$q_{e,exp}$ (mg·g^{-1})	Pseudo-first-order rate equation			Pseudo-second-order rate equation		
		k_1 (min^{-1})	$q_{e,cal}$ (mg·g^{-1})	R^2	k_2 (g·mg^{-1} min^{-1})	$q_{e,cal}$ (mg·g^{-1})	R^2
10	50.0000	0.0845	7.3790	0.8320	0.0267	50.5306	0.9999
40	198.7234	0.1340	223.9752	0.8729	0.0014	208.7683	0.9984
100	402.3404	0.0508	271.5189	0.9891	0.0003	440.5286	0.9994

where q_e is the amount adsorbed at equilibrium (mg g^{-1}), and C_e is the equilibrium concentration (mg L^{-1}). q_m is the maximum adsorption capacity (mg g^{-1}), and b is the Langmuir affinity constant related to the binding strength (L mg^{-1}). n and K_F are constants related to the adsorption intensity and capacity, respectively.

As shown in Fig. 3 and Table 3, the Langmuir model better fits the adsorption isotherms of CR on ZIF-8 than does the Freundlich model, and this suggests that there is a monolayer adsorption. Furthermore, the value of q_e for ZIF-8 decreased with an increase in temperature from 25°C to 45°C (Fig. 3(a)). The value of q_m was calculated to be 775 mg g^{-1} at 25°C. The CR maximum adsorption is compared with that of some reported adsorbents (Table 4) [4,12–15] to demonstrate the better performance of ZIF-8, and it can be seen that the ZIF-8 adsorption capacity is higher than that of most reported adsorbents.

3.4. Adsorption thermodynamics

Thermodynamics parameters, including the changes in Gibbs free energy ($\Delta G°$), enthalpy ($\Delta H°$), and entropy ($\Delta S°$), were used to evaluate the thermodynamics behavior of CR adsorption onto ZIF-8. The changes in $\Delta G°$, $\Delta H°$, and $\Delta S°$ were calculated from the following equations:

$$\Delta G° = \Delta H° - T\Delta S° \tag{6}$$

$$\Delta G° = -RT\ln K_d \tag{7}$$

$$K_d = \frac{q_e}{C_e} \tag{8}$$

Table 2
Parameters of intraparticle diffusion for CR adsorption on ZIF-8 at different temperatures

Temperature (°C)	Intraparticle diffusion					
	K_1 (mg g^{-1}·min$^{-1/2}$)	R^2	K_2 (mg g^{-1}·min$^{-1/2}$)	R^2	K_3 (mg g^{-1}·min$^{-1/2}$)	R^2
25	3.0744	0.9375	0.6691	0.8827	0.0024	0.0393
35	2.8820	0.9559	0.1975	0.5065	0.0391	0.0159
45	2.8415	0.9975	0.6087	0.7939	0.0391	0.0159

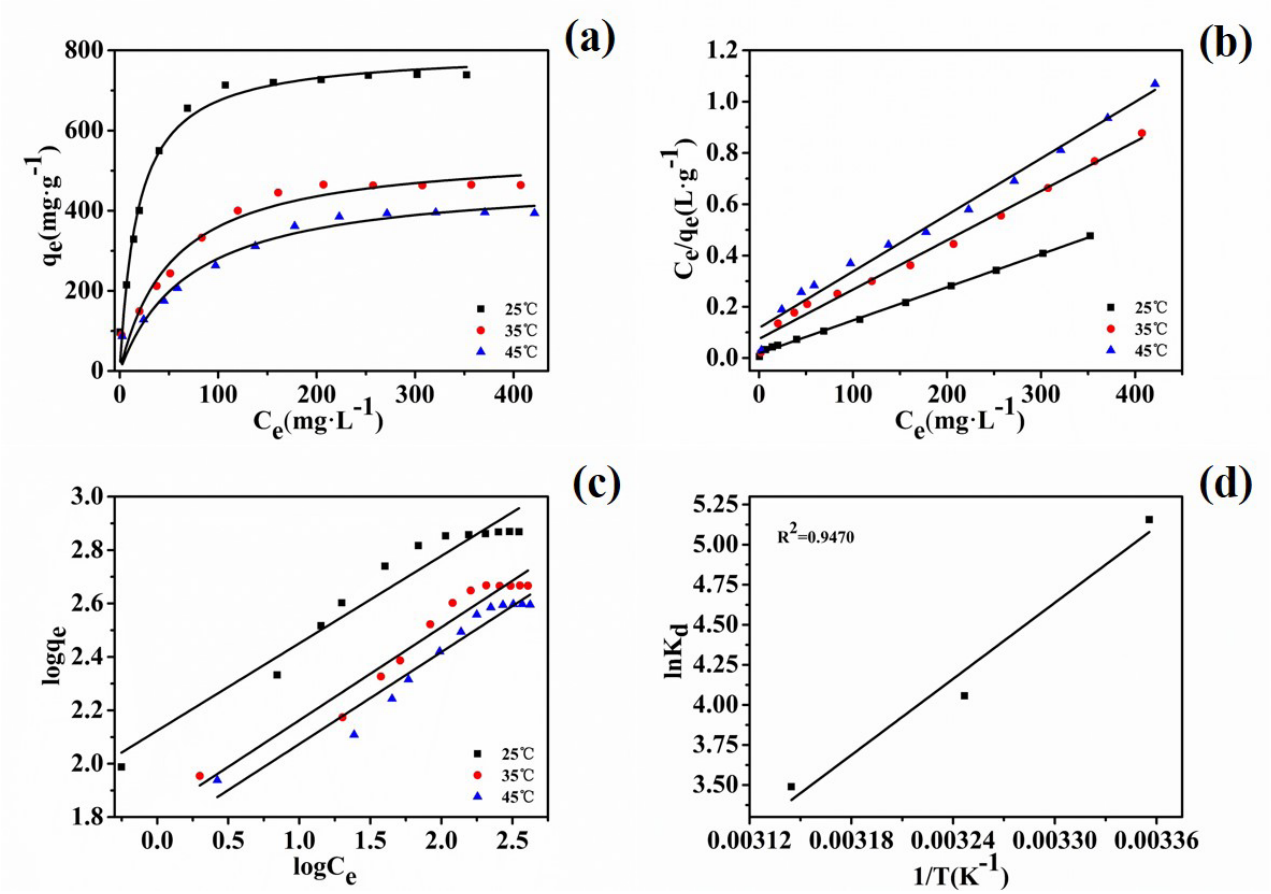

Fig. 3. (a) Adsorption isotherms, (b) Langmuir plots, (c) Freundlich plots, and (d) plot of lnK_d vs. 1/T for CR adsorption on ZIF-8.

Table 3
Fitting parameters of adsorption isotherms for CR adsorption on ZIF-8

Temperature (°C)	Langmuir			Freundlich		
	q_m (mg·g^{-1})	b (L·mg^{-1})	R^2	n	K_F ((mg·g^{-1})/(mg L^{-1})$^{1/n}$)	R^2
25	775.1938	0.0720	0.9986	3.0575	132.9872	0.9408
35	520.8333	0.0257	0.9887	2.8701	65.1884	0.9485
45	454.5455	0.0187	0.9836	2.9033	53.6105	0.9483

Table 4
Comparison of CR maximum adsorption capacities (Q_0) on various adsorbents

Type of adsorbent	Q_0 (mg/g)	Reference
ZIF-8	775	Present study
Bagasse fly ash (BFA)	11.885	Mall et al. [13]
Commercial grade activated carbons (ACC)	0.635	
Laboratory grade activated carbons (ACL)	1.875	
Ni50/Cu–BTC	1,078	Hu et al. [4]
Maghemite nanoparticles	208.33	Afkhami and Moosavi [12]
NiO/graphene nanosheets (NGNS)	123.89	Rong et al. [15]
Fe_3O_4@mTiO_2@GO	89.95	Li et al. [14]

$$\ln K_d = \frac{\Delta S^\circ}{R} - \frac{\Delta H^\circ}{RT} \quad (9)$$

R is the universal gas constant (8.314 J mol^{-1} K^{-1}), T is the temperature (K), and K_d is the distribution coefficient for the adsorption. The values of ΔH° and ΔS° can be obtained from the slope and the intercept, respectively, of the plots of $\ln K_d$ vs. $1/T$ (Fig. 3(d)). The obtained thermodynamics parameter values are shown in Table 5. The value of ΔG° for the adsorption at all temperatures was negative, and this indicates that the adsorption process is spontaneous. The decrease in the values of ΔG° with an increase in temperature indicates little feasibility for adsorption at higher temperatures. The negative value of ΔH° suggests that the adsorption is an exothermic reaction, which is in accordance with a decrease in the adsorption capacity associated with an increase in the adsorption temperature. Also, the negative value of ΔS° suggests decreased randomness at the adsorbent–solution interface during the adsorption process, and the negative value of ΔS° indicates that the mobility of CR onto the surface of ZIF-8 became more restricted in aqueous solution. This result showed that the driving force of CR adsorption on ZIF-8 was because of an enthalpy change rather than an entropy effect.

3.5. Effect of the solution pH

Fig. 4 shows a scheme of CR dye. The effect of solution pH on CR removal using ZIF-8 was investigated over a range of pH from 2 to 11 (Fig. 5(a)). The adsorption capacity significantly increased when the pH of the solution increased from 2 to 6 and decreased when the pH of the solution increased from 8 to 11. The maximum adsorption capacity was at neutral pH. To understand the reason for such behavior, the pH-dependent zeta potential curve of ZIF-8 is shown in Fig. 5(b). The point of zero charge for ZIF-8 was determined to be 9.4. CR is negatively charged at pH > 5.5, whereas it is positively charged at pH below 5.5 because of the protonated amino groups of CR [14]. For pH lower than 5.5, the positive charge on ZIF-8 electrostatically repels CR. For pH higher than 5.5, an electrostatic attraction between the positively charged ZIF-8 and negatively charged CR occurs, and this explains the better adsorption performance at neutral pH. For even higher solution pH, the number of positively charged sites on ZIF-8 decreased, and the negatively charged sites increased. These negatively charged sites do not favor the adsorption of dye anions because of electrostatic repulsion.

Fig. 5(c) shows XRD patterns of ZIF-8, and it can be seen that the crystallinity of ZIF-8 nanoparticles are retained well over pH = 2–11. It is worth noting that the crystallinity of ZIF-8 nanoparticles is also retained very well after CR adsorption, although the intensity of the adsorbed ZIF-8 nanoparticles is slightly lower than that of the virgin ZIF-8 nanoparticles. This decrease might be caused by the adsorbed CR on the surface of the ZIF-8 nanoparticles. In contrast, we observed an additional peak at 11.02° after the material was immersed in solution at pH = 2–11 for 120 min followed by CR adsorption. This could be because the water molecules are adsorbed on ZIF-8 nanoparticles and form some new crystal phases [16].

3.6. Effects of ionic strength

NaCl and $CaCl_2$ solutions with concentrations varying from 10 to 100 mM were used separately to adjust the solution salinity to evaluate the effects of ionic strength on the removal efficiency of the dye. As shown in Fig. 5(d), the adsorption capacity for CR increased to a certain value and then slightly decreased with an increase in the salt concentration. The removal increased obviously with an increase in the NaCl concentration from 0 to 40 mM and in the $CaCl_2$ concentration or 0 to 20 mM. However, CR removal decreased slightly when the ionic strength of NaCl increased from 40 to 100 mM and when that of $CaCl_2$ increased from 20 to 100 mM.

Table 5
Thermodynamics parameters for CR adsorption on ZIF-8

Temperature (°C)	$\Delta G°$ (kJ·mol^{-1})	$\Delta H°$ (kJ·mol^{-1})	$\Delta S°$ (J·mol^{-1}·K^{-1})
25	–12.7745	–65.8776	–178.8382
35	–10.3878		
45	–9.22422		

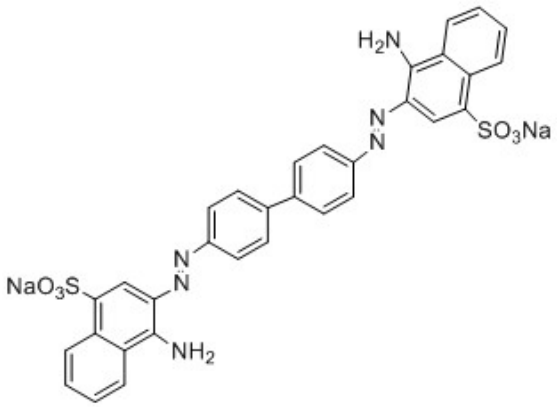

Fig. 4. Schematic diagram of CR dye.

There are generally two opposite effects that cause the impacts of ionic strength on the adsorption of CR. The salting-out effect promotes adsorption by decreasing the solubility of organic chemicals in the solution, thus enhancing hydrophobic interactions with the adsorbents [17]. In contrast, the invading effect of metal ions decreases adsorption via competition for adsorption space in the MOFs [18]. In the present study, low ion concentration could be more favorable for CR adsorption on ZIF-8 because of the salting-out effect that plays a leading role throughout the process. Adding ions can lead to competitive adsorption between anionic ions and CR. In contrast with monovalent Na^+, however, divalent Ca^{2+} has an incremental positive charge, and this increases repulsion with the positively charged ZIF-8, thereby the turning point appears at lower concentration.

3.7. Reusability of ZIF-8

Fig. 6(a) shows the reusability of the adsorbents, and this is a very important property for commercial feasibility. A slight loss of removal was observed on the regenerated materials for the three adsorption cycles, and this may result from some inactive sites being occupied by some CR molecules and thus complete desorption cannot be achieved. For an initial solution concentration of 40 mg/L and a ZIF-8 dosage of 0.2 g/L, after three adsorption cycles, 80% of removal efficiency was retained compared with the removal efficiency

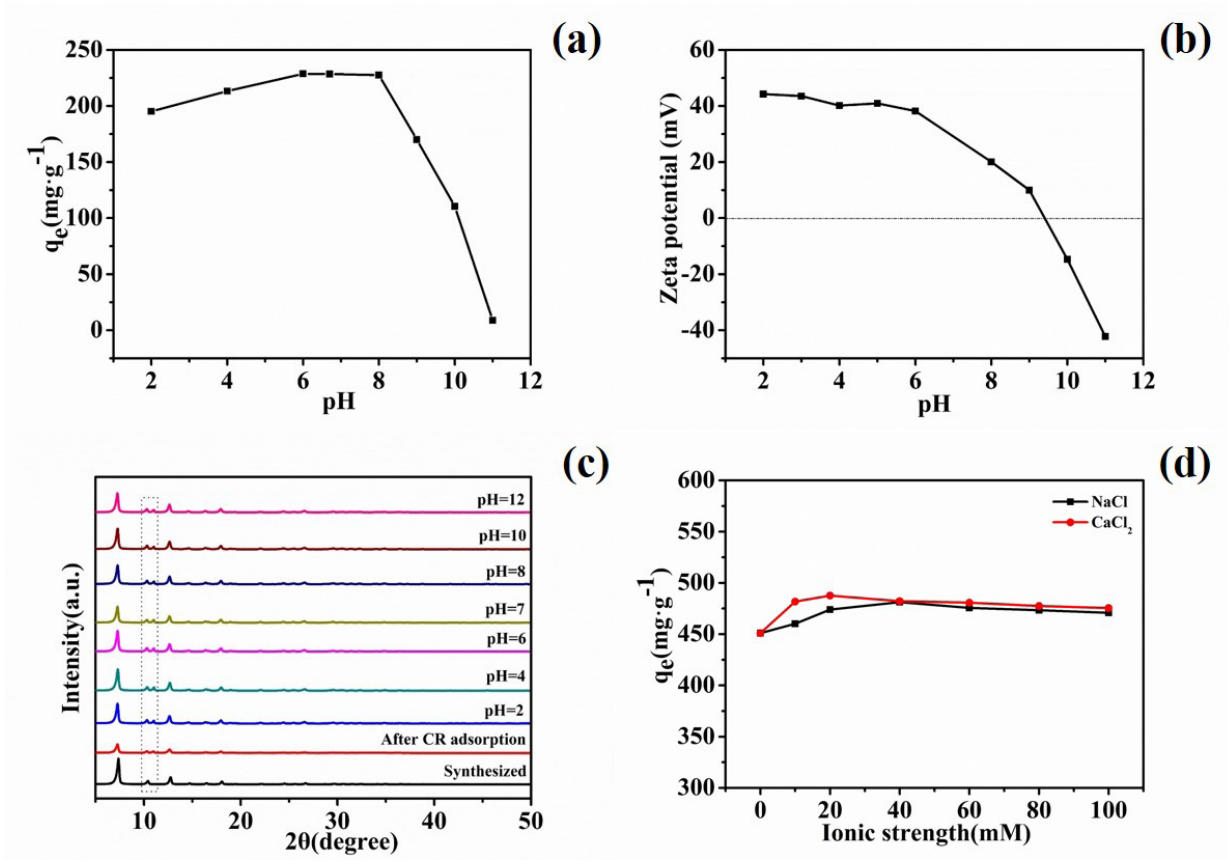

Fig. 5. (a) Effects of pH (C_o = 50 mg L^{-1}) and (d) ionic strength (C_o = 100 mg L^{-1}) on the CR adsorption on ZIF-8. (b) Zeta potential of ZIF-8 at various pH. (c) XRD of the synthesized ZIF-8 at different pH and of the used ZIF-8 after CR adsorption at pH = 6.7 (ZIF-8 = 0.2 g L^{-1}, t = 6 h, and T = 25°C).

of the fresh adsorbent, and this demonstrates the high regeneration capability of ZIF-8 and its good reusability for CR removal. The intact structure of the regenerated ZIF-8 was confirmed using XRD. Fig. 6(b) shows that there was no difference in the crystallinity of the original ZIF-8 nanoparticles and the thrice cycled ZIF-8 nanoparticles, and this indicates that the ZIF-8 structure has no significant change in adsorption after three cycles.

3.8. Adsorption mechanism

Pseudo-second-order kinetics and the Langmuir isotherm models matched well with the CR adsorption on ZIF-8. According to the three diffusion steps, it can be deduced that the present adsorption rates are mainly controlled by intraparticle diffusion. The thermodynamics analysis indicates that the system is spontaneous and exothermic and that the entropy increases. At the same time, the concentration of CR, the pH of the solution, and the ionic strength of the solution have different effects on ZIF-8 adsorption of CR. In addition to the concentration of CR, the pH of the solution, and the ionic strength of the solution, the surface properties of the adsorbent also have some impacts on CR adsorption by ZIF-8. From Figs. 1(c) and (d), the BET specific surface area, total pore volume, and pore size of the synthesized ZIF-8 nanoparticles were 1,345 m^2/g, 0.57 cm^3/g, and 12–90 nm, respectively. The huge specific surface provides a large number of adsorption sites for CR. The molecular size of CR is predicted to be 2.29 nm × 0.82 nm × 0.60 nm, and so the pore sizes in ZIF-8 are accessible and useful for adsorbing CR. Generally, large surface areas, high porosity, and accessible large pore cavities or channels are particularly favorable for an adsorbent to remove organic compounds because of the pore-filling effect [18].

The FTIR spectra of ZIF-8 nanoparticles before and after CR adsorption are shown in Fig. 7. In the FTIR spectra of the virgin ZIF-8 nanoparticles (Fig. 7(c)), the bands in the spectral region of 600–1,500 cm^{-1} are associated with the entire ring stretching or bending vibration; the band at 420 cm^{-1} is ascribed to the Zn-N stretching vibration. There is an FTIR band at 3,410 cm^{-1} and a broad and strong absorption band at 3,140 cm^{-1} for the as-prepared ZIF-8. These two bands are assigned to free hydroxyl groups (3,410 cm^{-1}) and hydrogen bonded hydroxyl groups (3,140 cm^{-1}) [19]. The FTIR spectrum of CR (Fig. 7(a)) has peaks at 640 cm^{-1} for C–C bending vibrations, 698 cm^{-1} for C–H stretching vibrations for a disubstituted aromatic compound, 833 cm^{-1} for p-disubstituted ring vibrations, 1,062 cm^{-1} for S=O stretching vibrations of sulfonic acid, 1,360 cm^{-1} for C–N bending vibrations, 1,590 cm^{-1} for N=N stretching vibrations, and 3,460 cm^{-1} for N–H stretching vibrations of primary amines [17].

For the spectra of ZIF-8 after CR adsorption (Fig. 7(b)), the characteristic peaks of ZIF-8 were retained, and some new peaks appeared at 543, 829, 1,040, 1,370, and 1,580 cm^{-1}. The bands at 1,300 and 1,500 cm^{-1} correspond to the imidazole rings of ZIF-8 and were slightly broader, which was because of the π–π stacking interactions between the aromatic rings of the dye molecules and ZIF-8 [20]. A shift in the peaks of p-disubstituted ring vibrations (S=O, C–N, and N=N) of CR to higher or lower wavenumbers indicates complex forms between ZIF-8 and CR [21]. The intensity of the peaks corresponding to N–H and O–H stretching vibrations in the range of 3,100–3,600 cm^{-1} were clearly weaker, and the peaks in this region became smooth. These results indicate that hydroxyl and amine groups might be involved in the adsorption process. At 420 cm^{-1}, a new band appears and could be attributed to the Zn–O vibration after adsorption, suggesting

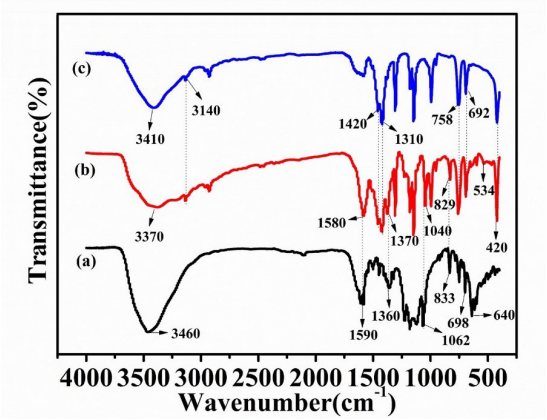

Fig. 7. FTIR spectra of (a) CR and ZIF-8 nanoparticles (c) before and (b) after CR adsorption.

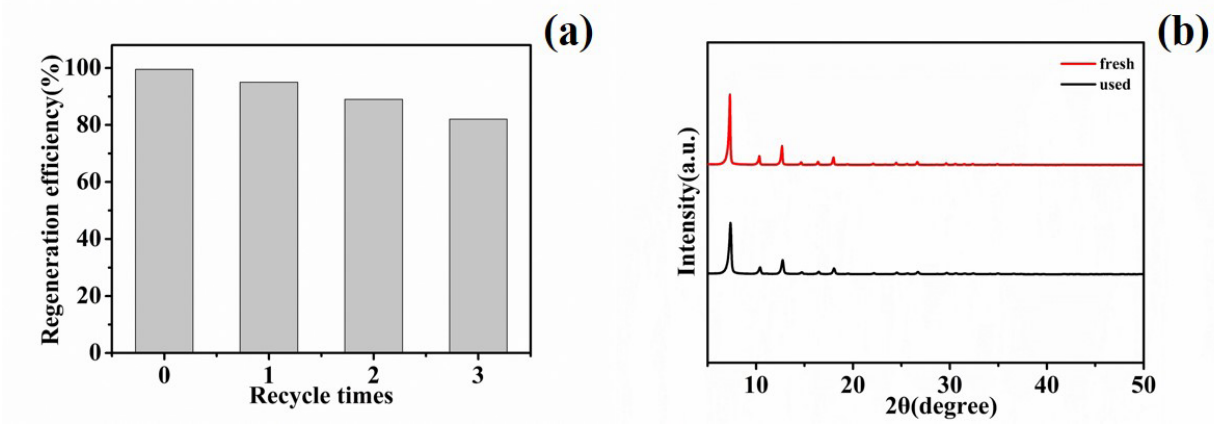

Fig. 6. (a) Recyclability of ZIF-8 for CR removal (ZIF-8 = 0.2 g L^{-1}, C_o = 40 mg L^{-1}, t = 6 h, pH = 6.7, and T = 25°C). (b) XRD patterns of ZIF-8 before and after three cycles regeneration.

that a complex with zinc is also formed. The obtained results show that the functional groups of ZIF-8 might be involved in the adsorption process and also confirm the adsorption is via π–π stacking interactions, electrostatic interactions, and hydrogen bonding.

XPS spectra of the key elements on the ZIF-8 surface before and after CR adsorption were recorded to better understand the adsorption mechanism. The Zn 2p, N 1p, O 1s, and S 2p narrow scans are shown in Fig. 8. Fig. 8(a) shows the Zn 2p spectra of the ZIF-8 nanoparticles before and after CR adsorption. The binding energies of 1,021.7 and 1,044.7 eV for the Zn 2p spectrum can be attributed to Zn 2p3/2 and Zn 2p1/2, respectively. After CR adsorption, the peak for Zn 2p is shifted to slightly higher binding energy, and the peak strength is slightly diminished. These observations imply that Zn is involved in CR sorption [8]. The N1s spectra are shown in Fig. 8(b). The binding energies at 398.8 and 399.3 eV are attributed to the N in the C=N– and C–NH– groups, respectively. After CR adsorption on the ZIF-8 nanoparticles, a new peak at 400.6 eV appears, and this peak is attributed to protonated nitrogen atoms being coordinated with CR sulfonic groups [22]. The O 1s spectra are shown in Fig. 8(c). The peaks with binding energies of 531.6 and 532.6 eV are assigned to O in the forms of Zn–OH and H_2O, respectively. Compared with the spectra of virgin ZIF-8, a new component peak with a binding energy of 530.8 eV was identified after CR adsorption, and these may possibly be assigned to Zn–O–S [23]. Also, the Zn–OH peak strength obviously diminishes, and the H_2O peak strength increases. These observations indicate that the Zn–OH bond is involved in the sorption process and that more water molecules are adsorbed on ZIF-8 nanoparticles. This is consistent with XRD results of ZIF-8 at different values of pH and of used ZIF-8 after CR adsorption at pH = 6.7 (Fig. 5(c)). As seen in Fig. 8(d), a new S 2p peak appeared in the spectra of the ZIF-8 nanoparticles after CR adsorption. The S 2p binding energies at 162.1 and 168.5 eV are ascribed to C–S– and $–SO_3^-$, respectively [24], and this clearly indicates the presence of CR on the sorption surface.

On the basis of the above analysis, it can be confirmed that the adsorptions proceed via several different mechanisms such as electrostatic attractions, pore-filling effect, π–π interactions, and hydrogen bonding interactions between ZIF-8 and CR (Fig. 9). The advantage of ZIF-8 for CR removal can be ascribed to electrostatic interactions and hydrogen bonding interactions. CR removal using ZIF-8 nanoparticles can be associated with the electrostatic attractions between protonated N atoms (e.g., $C=NH^+–$ and $C–NH_2^+–$) or Zn–OH and $–SO_3–$ of CR and can be associated with surface complexation via hydrogen bonding between the oxygen atoms in CR functional groups and the amine group of ZIF-8 [1,3,8]. In addition, the activated sites, Zn–OH, and the amine groups of ZIF-8 can hydrogen bond with CR nitrogen or oxygen atoms.

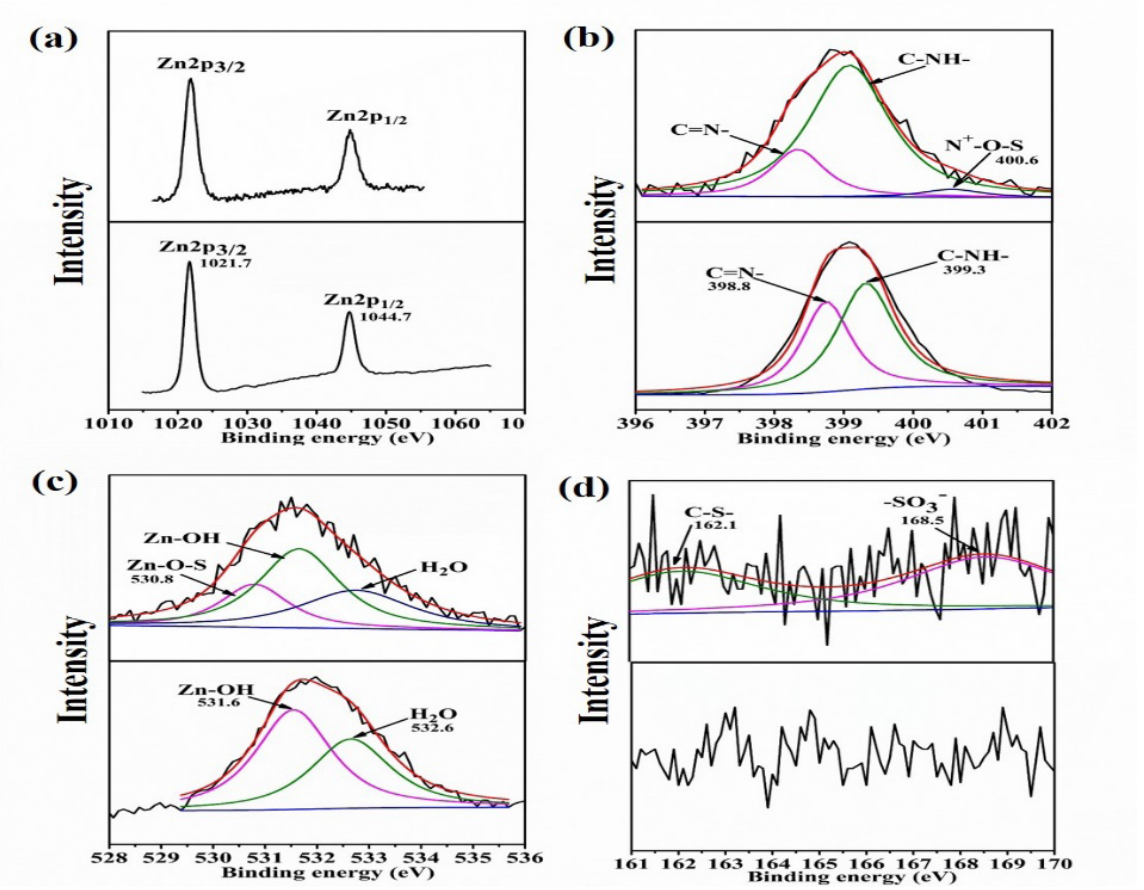

Fig. 8. XPS spectra for (a) Zn 2p, (b) N 1s, (c) O 1s, and (d) S 2p of ZIF-8 nanoparticles before (top panels of (a)–(d)) and after (bottom panels of (a)–(d)) CR adsorption.

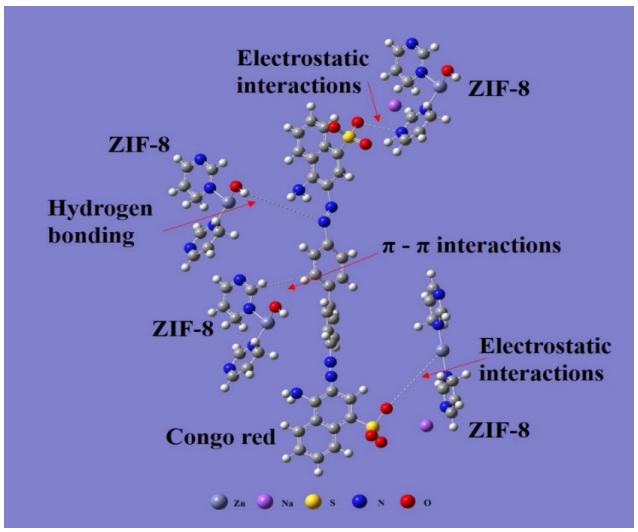

Fig. 9. Proposed binding mechanism for CR adsorption on ZIF-8.

4. Conclusion

In this study, ZIF-8 nanoparticles were synthesized for the adsorption removal of CR from water via a facile method at room temperature. The synthesized ZIF-8 nanoparticles had an average size of 73 nm, had a microporous structure with a high surface area of 1,345 m^2/g, and demonstrated efficient adsorptive CR removal. The adsorption is affected by solution pH, initial dye concentration, temperature, contact time, and ionic strength. The pseudo-second-order kinetics and Langmuir isotherm models matched well with CR adsorption on ZIF-8. The maximum equilibrium adsorption capacity was 775 mg g^{-1}. The thermodynamics analysis indicates that the system is spontaneous and exothermic and that the entropy increases. XPS and FTIR analysis showed that the adsorption processes may involve electrostatic attractions, the pore-filling effect, π–π interactions, and hydrogen bonding interactions between ZIF-8 and CR.

Acknowledgments

This work was financed by the National Natural Science Foundation of China (No. U1401235), the Applied Science and Development Project of Guangdong Province (No. 2016B020240005) and the Central University of basic scientific research business funded projects (No. D2172D068).

References

[1] F. Zhang, X. Yin, W. Zhang, Development of magnetic $Sr_5(PO_4)_3(OH)/Fe_3O_4$ nanorod for adsorption of Congo red from solution, J. Alloys Compd., 657 (2016) 809–817.
[2] T.M. Rao, V.V.B. Rao, Biosorption of Congo Red from aqueous solution by crab shell residue: a comprehensive study, SpringerPlus, 5 (2016) 537–544.
[3] Y. Zhang, L. Bai, W. Zhou, R. Lu, H. Gao, S. Zhang, Superior adsorption capacity of Fe_3O_4 @$nSiO_2$ @$mSiO_2$ core-shell microspheres for removal of congo red from aqueous solution, J. Mol. Liq., 219 (2016) 88–94.
[4] J. Hu, H. Yu, W. Dai, X. Yan, X. Hu, H. Huang, Enhanced adsorptive removal of hazardous anionic dye "congo red" by a Ni/Cu mixed-component metal–organic porous material, RSC Adv., 4 (2014) 35124–35130.
[5] H. Yu, T. Wang, L. Yu, W. Dai, N. Ma, X. Hu, Y. Wang, Remarkable adsorption capacity of Ni-doped magnolia-leaf-derived bioadsorbent for congo red, J. Taiwan Inst. Chem. Eng., 64 (2016) 279–284.
[6] N.A. Khan, B.K. Jung, Z. Hasan, S.H. Jhung, Adsorption and removal of phthalic acid and diethyl phthalate from water with zeolitic imidazolate and metal-organic frameworks, J. Hazard. Mater., 282 (2015) 194–200.
[7] S. Zhao, D. Chen, F. Wei, N. Chen, Z. Liang, Y. Luo, Removal of Congo red dye from aqueous solution with nickel-based metal-organic framework/graphene oxide composites prepared by ultrasonic wave-assisted ball milling, Ultrason. Sonochem., 39 (2017) 845–852.
[8] M.T. Thanh, T.V. Thien, V.T.T. Chau, P.D. Du, N.P. Hung, D,Q. Khieu, Synthesis of iron doped zeolite imidazolate framework-8 and its remazol deep black RGB dye adsorption ability, Jordan J. Chem., 2017 (2017) 18–27.
[9] J. Cravillon, S. Münzer, S.J. Lohmeier, A. Feldhoff, K. Huber, M. Wiebcke, Rapid room-temperature synthesis and characterization of nanocrystals of a prototypical zeolitic imidazolate framework, Chem. Mater., 21 (2009) 1410–1412.
[10] M. Jian, B. Liu, G. Zhang, R. Liu, X. Zhang, Adsorptive removal of arsenic from aqueous solution by zeolitic imidazolate framework-8 (ZIF-8) nanoparticles, Colloids Surf., A, 465 (2015) 67–76.
[11] B.K. Jung, J.W. Jun, Z. Hasan, S.H. Jhung, Adsorptive removal of p-arsanilic acid from water using mesoporous zeolitic imidazolate framework-8, Chem. Eng. J., 267 (2015) 9–15.
[12] A. Afkhami, R. Moosavi, Adsorptive removal of Congo red, a carcinogenic textile dye, from aqueous solutions by maghemite nanoparticles, J. Hazard. Mater., 174 (2010) 398–403.
[13] I.D. Mall, V.C. Srivastava, N.K. Agarwal, I.M. Mishra, Removal of congo red from aqueous solution by bagasse fly ash and activated carbon: kinetic study and equilibrium isotherm analyses, Chemosphere, 61 (2005) 492–501.
[14] L.L. Li, X.J. Li, H.M. Duan, X.J. Wang, C.N. Luo, Removal of Congo Red by magnetic mesoporous titanium dioxide-graphene oxide core-shell microspheres for water purification, Dalton Trans., 43 (2014) 8431–8438.
[15] X. Rong, F. Qiu, J. Qin, H. Zhao, J. Yan, D. Yang, A facile hydrothermal synthesis, adsorption kinetics and isotherms to Congo Red azo-dye from aqueous solution of NiO/graphene nanosheets adsorbent, J. Ind. Eng. Chem., 26 (2015) 354–363.
[16] G. Yuan, G. Zhang, Y. Zhou, F. Yang, Synergetic adsorption and catalytic oxidation performance originating from leafy graphite nanosheet anchored iron(ii) phthalocyanine nanorods for efficient organic dye degradation, RSC Adv., 5 (2015) 26132–26140.
[17] A.A. Telke, S.M. Joshi, S.U. Jadhav, D.P. Tamboli, S.P. Govindwar, Decolorization and detoxification of Congo red and textile industry effluent by an isolated bacterium *Pseudomonas* sp., SU-EBT, Biodegradation, 21 (2009) 283–296.
[18] X.F. Chen, H. Zang, X. Wang, J.G. Cheng, R.S. Zhao. C.G. Cheng, X.Q. Lu, Metal–organic framework MIL-53 (Al) as a solid-phase microextraction adsorbent for the determination of 16 polycyclic aromatic hydrocarbons in water samples by gas chromatography–tandem mass spectrometry, Analyst, 137 (2012) 5411–5419.
[19] X. Zhu, Y. Liu, G. Luo, F. Qian, S. Zhang, J. Chen, Facile fabrication of magnetic carbon composites from hydrochar via simultaneous activation and magnetization for triclosan adsorption, Environ. Sci. Technol., 48 (2014) 5840–5848.
[20] M. He, J. Yao, Q. Liu, K. Wang, F. Chen, H. Wang, Facile synthesis of zeolitic imidazolate framework-8 from a concentrated aqueous solution, Microporous Mesoporous Mater., 184 (2014) 55–60.
[21] S. Dhanavel, E.K.A. Nivethaa, K. Dhanapal, V.K. Gupta, V. Narayanan, A. Stephen, α-MoO_3/polyaniline composite for effective scavenging of Rhodamine B, Congo red and textile dye effluent, RSC Adv., 6 (2016) 28871–28886.
[22] Y. Li, R. Cao, X. Wu, J. Huang, S. Deng, X. Lu, Hypercrosslinked poly(styrene-co-divinylbenzene) resin as a specific polymeric adsorbent for purification of berberine hydrochloride from aqueous solutions, J. Colloid Interface Sci., 400 (2013) 78–87.
[23] S. Deng, G. Yu, S. Xie, Q. Yu, J. Huang, Y. Kuwaki, Enhanced adsorption of arsenate on the aminated fibers sorption behavior and uptake mechanism, Langmuir, 24 (2008) 10961–10967.
[24] Y. Sun, Y. Wu, H. Shan, G. Wang, C. Li, Studies on the promoting effect of sulfate species in catalytic dehydrogenation of propane over Fe_2O_3/Al_2O_3 catalysts, Catal. Sci. Technol., 5 (2015) 1290–1298.